Solar Energetic Particle Driven Alfvén Wave Growth and Consequences

Chee K. Ng,[1,2] Donald V. Reames,[1] and Allan J. Tylka[3]
(1) Code 661, NASA Goddard Space Flight Center, Greenbelt, MD 20771, USA
(2) Dept of Astronomy, University of Maryland, College Park, MD 20742, USA
(3) Code 7652, Naval Research Laboratory, Washington DC 20375-5352, USA

Abstract

Our model shows that in large solar energetic particle (SEP) events, streaming protons amplify interplanetary (IP) Alfvén waves by orders of magnitude near the Sun. The wave intensity varies strongly and non-monotonically in wavenumber, time, and space. It falls steeply with distance and may be difficult to observe at 1 AU. Wave amplification dynamically modifies the rigidity and radial dependence of SEP scattering and throttles SEP transport. It is essential in understanding the time and energy variations of SEP elemental abundances.

1. Model

SEPs from a traveling IP shock and Alfvén waves interact via quasilinear resonance. The phase-space densities f_s of s-species ions and magnetic intensity I^σ of outward, circularly polarized Alfvén waves (σ = R+,L+) are governed by:

$$\frac{\partial f_s}{\partial t}+(\mu v+V_{\rm sw})\frac{\partial f_s}{\partial r}+\frac{1-\mu^2}{r}\left[(v+\mu V_{\rm sw})\frac{\partial f_s}{\partial \mu}-V_{\rm sw}P\frac{\partial f_s}{\partial P}\right]-\frac{\partial}{\partial \mu}\left[D_{\mu\mu}\frac{\partial f_s}{\partial \mu}\right]=g_s, \tag{1}$$

$$\frac{\partial}{\partial t}\left(\frac{V_{\rm wa}}{V_{\rm A}}I^\sigma\right)+\frac{1}{r^2}\frac{\partial}{\partial r}\left(r^2\frac{V_{\rm wa}^2}{V_{\rm A}}I^\sigma\right)-\frac{\partial}{\partial k}\left(k\frac{dV_{\rm wa}}{dr}\frac{V_{\rm wa}}{V_{\rm A}}I^\sigma\right)=\gamma_\sigma\frac{V_{\rm wa}}{V_{\rm A}}I^\sigma. \tag{2}$$

$$D_{\mu\mu}(\mu,v,P,r,t)=\sum_\sigma\frac{v^2}{4P^2}\int dk\, I^\sigma(k,r,t)R^\sigma_{\mu\mu}(\mu,v,P,k,V_{\rm A},B), \tag{3}$$

$$\gamma_\sigma(k,r,t)=2\pi^2cV_{\rm A}\sum_s Q_s^3e^3\iint d\mu dP\frac{P^3R^\sigma_{\mu\mu}}{\mathcal{E}^2(1-\mu V_{\rm A}/v)^2}\left[\frac{\partial f_s}{\partial \mu}-\frac{V_{\rm A}}{v}\left(\mu\frac{\partial f_s}{\partial \mu}-P\frac{\partial f_s}{\partial P}\right)\right]+\zeta_1. \tag{4}$$

$$g_s(r,P,t)=\frac{b\,n_s(r)\,(V_{\rm sh}-V_{\rm sw})\,(\alpha-3)}{4\pi P_{0,s}^3}\left(\frac{P}{P_{0,s}}\right)^{-\alpha}\exp\left(-\frac{evP}{2cE_e(r)}\right)\delta(r-r_{\rm sh}). \tag{5}$$

P is rigidity, μ pitch-cosine, t time, r radial distance, k wavenumber, $\mathcal{E}$ total particle energy, $R_{\mu\mu}$ resonance function, B mean magnetic field. $r_0\equiv 1\,$AU. Solar-wind ion density $n_s=n_{s,0}\,(r_0/r)^2$. $n_{\rm H,0}=5\,{\rm cm}^{-3}$, $n_{s,0}/n_{\rm H,0}$ = coronal values

pp. 3339–3342

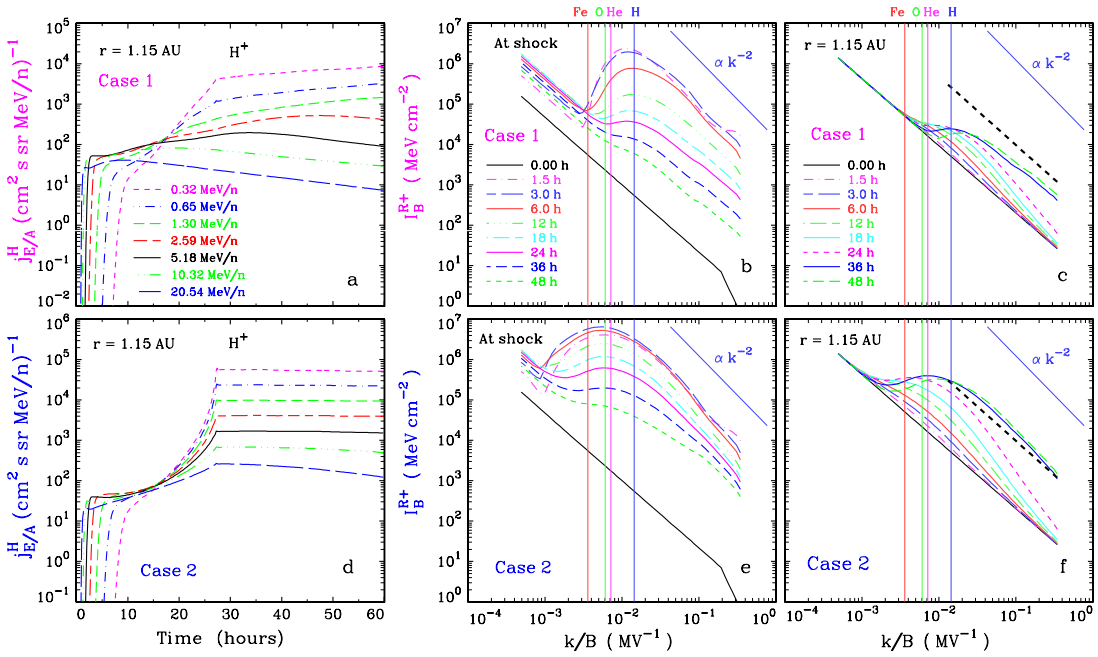

Fig. 1. Proton intensity histories at $r = 1.15$ AU and evolution of I^{R+} wave spectrum at the moving shock and at $r = 1.15$ AU. Top (bottom) panels are for Case 1 (2).

[4]. Alfvén speed $V_A = V_{A,0}\, r_0/r$, $V_{A,0} = 33.3$ km/s. Plasma speed $V_{sw} = 333$ km/s. $V_{wa} = V_A + V_{sw}$. Shock speed $V_{sh} = 1667$ km/s. Shock distance $r_{sh} = r_{sh,0} + V_{sh}t$, $r_{sh,0} = 13.4\, R_\odot$. Charge state $Q = 6.67$ for O and 13.88 for Fe. e-folding energy $E_e \propto Q/A$, $A =$ atomic mass, and $E_e = E_{e,0}\, r_0/r_{sh}$ for proton. Ion seed energy = 5 keV/amu. SEP source spectral index $\alpha = \alpha_0 + \alpha'(r_{sh} - r_{sh,0})$, $\alpha_0 = 4$. Full particle reflection at inner boundary $r_a = 10.7 R_\odot$. 95% reflecting outer boundary moves out with V_{sw} from $r_b = 2$ AU at $t = 0$. Ambient waves: magnetic intensity $I_0^{R+} = I_0^{L+} = 2500$ MeV cm^{-2} at r_0 and $k/B = 0.023$ MV^{-1}; spectral index $\delta = 1.667$; and change rate $\zeta_1 = -0.01$ hr^{-1}. We consider two cases. For Case 1 (2), $E_{e,0} =$ 60 (2000) MeV; $\alpha' = 2.5$ (0.5) AU^{-1}; and seed particle fraction $b = 0.005$ (0.0025).

At $t = 0$, $f_s \equiv 0$ and $I^\sigma =$ steady-state solution of eq. (2) for Alfvén waves from the Sun. At $t > 0$, SEPs are released at the moving shock (eq. (5)). Eqs. (1)-(2) are solved numerically for f_s and I^σ. See [3] for details.

2. Results

Fig. 1 illustrates the evolution of SEPs and IP Alfvén waves: the lower panels show for the longer and harder proton source in Case 2, SEP intensities rising to shock passage and wave growth extending to lower k/B. Wave growth is rapid and large near the shock at $r < 0.1$ AU (Fig. 1b,e) but slow and weak at r=1.15 AU (Fig. 1c,f), below or barely exceeding typical observed magnetic power

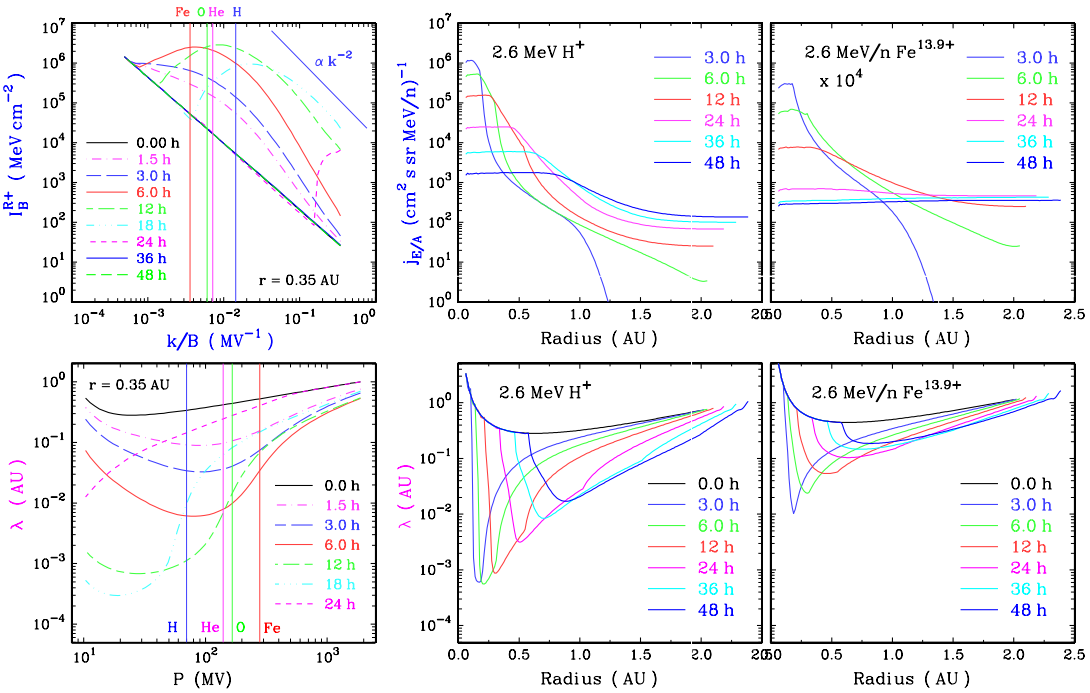

Fig. 2. For Case 1: Relating evolving I^{R+}-k/B to λ-P profiles at $r = 0.35$ AU (left panels). Vertical lines in the λ vs P panel give the rigidity of 2.6 MeV/amu ions.

spectrum [1] (black dashed line) as the shock approaches. The vertical lines in Fig. 1b,c,e,f give the resonant k/B for 2.6 MeV/amu $Fe^{+13.9}$, $O^{+6.7}$, He^{+2}, and H^{+} ions at $\mu = 1$. The resonant k/B ranges at $k/B \approx (|\mu|P)^{-1}$ move to the left with increasing energy, and to the right and broaden as $|\mu|$ decreases.

The proton-amplified waves greatly modify SEP transport by changing the P- and r-dependence of particle scattering. As depicted for Case 1 at $r = 0.35$ AU, the wave spectra grow non-uniformly (Fig. 2 upper left) and carve a deep valley in the λ-P profile (λ = mean free path) (Fig. 2 bottom left), creating non-monotonic P and A/Q dependence in SEP transport. Comparing the j_E-r and λ-r profiles (Fig. 2 middle or right panels) demonstrate vividly the powerful control of the amplified waves on the outward transport of 2.6 MeV/amu H^{+} or $Fe^{+13.9}$ ions.

Fig. 3 displays Fe/O and He/H vs t at $r = 1.15$ AU. Because Case 1 has few > 60 MeV protons, the amplified wave spectrum falls steeply at $k/B < 0.01$ MV^{-1}. The vertical lines in Fig. 1b,e help us to deduce that the scattering-rate ratio of O to Fe at 2.6 MeV/amu rises higher in Case 1 than in Case 2 as the waves intensify, leading to a higher 2.6 MeV/amu Fe/O rebound (Fig. 3 top left). At 0.32 MeV/amu, Fe/O rises from < 1 because λ decreases with P at the relevant rigidities (Fig. 2 bottom left). Fig. 3 top right and bottom right panels show that for both Case 1 and 2, the energy spectra of 24-hr averaged ratios of He/H and Fe/O depart only marginally from the spectra of He/H and Fe/O source ratios.

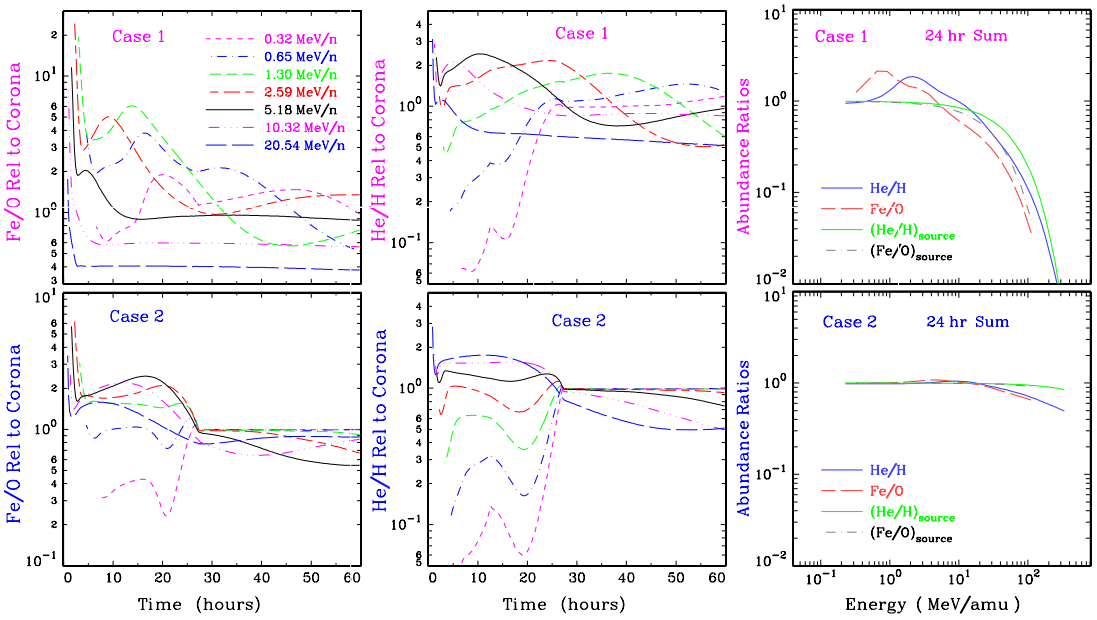

Fig. 3. Fe/O and He/H histories and 24-hr summed energy spectra at $r = 1.15$ AU.

The observed Fe/C upturn at > 30 MeV/amu in the 2000 July 14 event was attributed to shock acceleration of impulsive remnant suprathermals [5].

3. Discussion and Conclusion

We described above some important effects of wave amplification, which is required by energy conservation when waves scatter SEPs. As the amplified waves propagate out, B falls and k/B rises, thus freeing higher rigidity SEPs from their control. The amplified waves give $\lambda \propto r^{-4}$ at $t < 3$ hr and $r < 0.3$ AU (Fig. 2 bottom middle panel). Peak SEP intensity $\propto r^{-3}$, focusing strength and $V_A \propto r^{-1}$ all contribute to the strong λ-r (and I^{σ}-r) dependence. Wave amplification was successfully used to model observed time variations of SEP abundances [e.g., 2,6]. It is essential when we extend such studies to a broader energy range and in studying species dependence in shock acceleration.

4. References

1. Leamon, R. J. 1998, J. Geophys. Res. 103, 4775
2. Ng, C. K., Reames, D. V., Tylka, A. J. 1999, GRL 26, 2145
3. Ng, C. K., Reames, D. V., Tylka, A. J. 2003, ApJ (in press)
4. Reames, D. V. 1999, Space Sci. Rev. 90, 413
5. Tylka, A. J. 2001, ApJ 558, L59.
6. Tylka, A. J., Reames, D. V., Ng, C. K. 1999, GRL 26, 2141